Magnetic damping in ferromagnetic/heavy-metal systems: The role of interfaces and the relation to proximity-induced magnetism

C. Swindells,[1,2] H. Głowiński,[3] Y. Choi,[4] D. Haskel,[4] P. P. Michałowski,[5] T. Hase,[6] F. Stobiecki,[3] P. Kuświk,[3] and D. Atkinson[1,*]

[1]*Department of Physics, Durham University, South Road, Durham DH1 3LE, United Kingdom*
[2]*Department of Material Science and Engineering, University of Sheffield, Sheffield S1 3JD, United Kingdom*
[3]*Institute of Molecular Physics, Polish Academy of Sciences, Smoluchowskiego 17, 60-179 Poznań, Poland*
[4]*Advanced Photon Source, Argonne National Laboratory, Argonne, Illinois 60439, USA*
[5]*Łukasiewicz Research Network - Institute of Microelectronics and Photonics, Aleja Lotników 32/46, 02-668 Warsaw, Poland*
[6]*Department of Physics, University of Warwick, Coventry CV4 7AL, United Kingdom*

(Received 17 December 2021; accepted 15 March 2022; published 25 March 2022)

Damping and spin transport in spintronic multilayered systems continues to be a topic of active research. The enhancement of damping in ferromagnet (FM)/spacer layer (SL)/heavy-metal (HM) thin-film systems was studied for $Co_{25}Fe_{75}$/SL/Pt with a nonmagnetic (NM) SL of either Au or Cu with variable thickness, in order to understand the correlation with proximity-induced magnetism (PIM) in the HM. Structural, PIM and magnetic damping measurements were undertaken on the same samples. Specifically, secondary ion mass spectroscopy, element specific x-ray magnetic reflectivity and x-ray magnetic circular dichroism at the Pt and Au L_3 edges, and ferromagnetic resonance methods were used. With increasing thickness of a Cu or Au SL directly between the FM and the Pt layer, the Pt PIM and the damping both fall rapidly, with a relationship between damping and PIM that depends on the SL material. The PIM observed in the Au layer showed a complex dependence on the layer thickness, suggesting some hybridization with the Pt. The role of the number and location of interfaces on the damping was demonstrated with the addition of a SL within the Pt layer, which showed that the specific details of the NM/HM interface also affects the damping. The insertion of a Cu SL within the Pt showed a measurable increase in the overall enhancement of the damping while the insertion of a Au SL into Pt had almost no effect on the damping. Together these results demonstrate the role of both PIM and of additional interfaces in the enhancement of damping in FM/HM systems, which is not fully accounted for by existing theory.

DOI: 10.1103/PhysRevB.105.094433

I. INTRODUCTION

The interface between ferromagnetic (FM) and nonmagnetic (NM) materials hosts a wide range of useful physical phenomena that underpin current and future spintronic technologies. A key theme in spintronics is the propagation of spin current between different layers. This may be from a FM into a NM layer, leading to an enhancement of the ferromagnetic damping, or a spin current generated via the spin Hall effect in a heavy metal flowing into a ferromagnetic layer and resulting in a spin-orbit torque (SOT). Such interfacial spin transport depends critically upon the details of the interface [1–6], but there are questions about its dependence on the location and number of interfaces. Furthermore, the role of the proximity-induced moment (PIM) of the HM on damping and spin transport has been a subject of debate [7–10].

This paper details a systematic study of the effects of proximity-induced magnetic polarization and the role of different nonmagnetic spacer layers on ferromagnetic damping in FM/NM systems. The results are discussed in the context of spin pumping and diffusive spin current in FM/NM systems.

For heavy metals (HM) close to the Stoner criterion, such as Pt and Pd, it is known that hybridization at the interface with a transition-metal FM leads to a proximity-induced moment [11–14]. This moment has been observed experimentally, using element specific x-ray magnetic circular dichroism (XMCD), in nonmagnetic materials either alloyed with [15–17] or at the interface with [18–20] ferromagnetic transition metals (TMs), where a decrease observed in the TM moment was accompanied by an increase in the Pt moment [13]. Though some debate remains regarding the presence [21,22], or absence [21,23,24] of PIM in Pt layered with different transition-metal-oxide ferrimagnets, more recently, PIM in Pt layered with rare earth–TM ferrimagnets was demonstrated and shown to be aligned with the orientation of the transition metal, regardless of the net ferrimagnetic moment direction [25].

The interfacial nature of the induced moment in Pt layered with ferromagnetic thin films implies a limited spatial extent which was established using XMCD in studies with stepwise Pt thickness variations [13,26], while more recent detailed studies using x-ray resonant magnetic reflectivity (XRMR) have shown the spatial distribution of the PIM can be mapped through a single Pt layer [27,28]. It has also been shown that the magnitude of the PIM is constant above a threshold thickness [29] and is dependent upon the interface quality

*del.atkinson@durham.ac.uk

[30]. In the latter case, a larger total Pt PIM was commonly observed at the FM/Pt interface compared to a Pt/FM interface [25,28,31,32]. In all these studies the spatial variation of the induced moment has been shown, or assumed, to be closely confined to the interface as it is intimately associated with local FM/HM electronic hybridization.

Returning to damping, a widely used physical description for the enhancement of magnetic damping in FM/NM systems involves the flow of spin current into a NM layer from spin accumulation generated by precession in the FM, termed spin pumping, that was developed by Tserkovnyak *et al.* on the basis of scattering theory [33–38]. In this theoretical framework, precessing magnetization within a FM layer creates an unbalanced electrochemical potential at the interface between the FM and NM layers that leads to the accumulation of one spin state at the interface. This nonequilibrium spin accumulation is the source of spin current that propagates into the NM layer [38]. The magnitude of the spin current depends on the NM material parameters and the details of the interface itself, specifically the matching of the conductance channels. Heavy metals, such as Pt, are referred to as good *spin sinks*, as their large spin-orbit coupling (SOC) gives rise to a short spin-diffusion length λ_{sd} resulting in the spin currents dissipating quickly inside the NM layer. In spin-pumping theory any static PIM of the NM metal is not explicit in the description of the transmission of spin current across an interface, as the computed Sharvin conductance is mostly unchanged, even for ultrathin films [36]. Furthermore, Tserkovnyak *et al.* also state the nonequilibrium spin accumulation, which drives the spin current, is unaffected by the Stoner enhancement through equilibrium polarization, although the proximity spin density is enhanced.

An alternative description for the enhancement of Gilbert damping with interfaces between FM and NM layers is based on a tight-binding model developed by Barati *et al.* [39] that builds upon the damping mechanism defined by Kamberský [40], which considers magnon relaxation with inter- and intraband transitions arising from SOC [41]. For materials such as Pd and Pt the damping contribution is large due to the large SOC and the opportunity for orbital hybridization from the *d*-band crossing the Fermi level with a large spin-split density of states [39]. This hybridization is also responsible for the proximity-induced moment in HMs [13] and hence the Barati *et al.* approach provides a theoretical basis for linking damping and PIM.

The influence of proximity-induced magnetization on damping has thus far produced contrasting conclusions in experimental studies, with reports claiming proximity-induced magnetization has a profound effect [8] or no effect at all [9,42] on interfacial spin-transport phenomena. Debate also remains as to how to treat the parameters of interest, such as the HM spin diffusion length, with some approaches dividing the HM into two regions [43], and others stating that although PIM is not explicitly included in the mathematical description of spin pumping, it ultimately affects the resultant spin transport, by effectively shortening the spin diffusion length of the HM, via dephasing of the spin current [44].

The role of PIM in spin-pumping experiments has typically been studied by inserting a thin spacer layer (SL) at the interface between the FM and HM. Such studies have shown a reduction in damping with a SL, for example with Al [45], which was attributed to a loss of PIM in the HM. More commonly in spintronics, Cu and Au have been used as the SL as both have a large spin diffusion length, which, in principle, presents a quasitransparent layer to the spin current (λ_{sd} for Cu being ∼100 nm [46–49] and ∼60 nm for Au [50]). Indeed, Cu spacer layers were shown to have little effect on the measured spin Hall angle in Co/Cu/Pt [2], which was attributed to the long spin diffusion length and the low SOC of Cu. Surprisingly, a XMCD study showed a large decrease in the additional damping linked to spin pumping when a thin Cu spacer layer was inserted between the FM and HM layers that was attributed to a decrease in the HM PIM [8]. The situation is further complicated by reports of an induced moment in ultrathin (<0.4 nm) Cu between perpendicularly magnetized Co/Pt layers [51].

It must also be recognized that the location of a SL layer within a multilayered system and the structure and electronic interactions of the resulting interfaces are also critical. Interfacial regions are finite due to a combination of roughness and intermixing [52,53] and these details influence the electronic behavior at the interface. It is thus helpful to compare interface width and compositional intermixing, with the magnitude and spatial extent of any proximity-induced moment both within the main HM layer, but also in the spacer layer material, and to relate this to the resulting damping and analysis of spin transport.

This paper presents a systematic experimental investigation that aims to inform on damping in relation to PIM of Pt in the system, the effect of different nonmagnetic spacer layer materials, and the location and number of SL interfaces within the FM/HM system. Cu and Au were chosen as SL materials on the basis of their large spin diffusion length. Damping was investigated using ferromagnetic resonance (FMR) and discussed in terms of spin pumping. Pt PIM in FM/SL/Pt system was studied using element specific synchrotron XRMR and XMCD measurements as a function of Cu or Au SL thickness. PIM in the Au SL was also studied by the same methods. Structural information was obtained from both the analysis of x-ray reflectivity (XRR) and element specific secondary ion mass spectroscopy (SIMS). The relationships between the structural profiles at the interface, the PIM in Pt and Au, and the damping were investigated. For clarity the results are presented separately for the Cu and Au SL systems, then the results are brought together in the discussion.

II. METHODS AND CHARACTERIZATION

Samples were grown using magnetron sputtering with an Ar^+ ion process gas on thermally oxidized Si substrates. Multilayers consisted of a $Co_{25}Fe_{75}$ FM layer, Pt as the heavy-metal "spin sink," and either Cu or Au as the SL. The CoFe layer was deposited onto a Cu buffer, as this was previously shown to give low initial damping for the CoFe [54]. To investigate the thickness dependencies, a thickness gradient of either the SL or the Pt layer was deposited in one lateral dimension along the sample over a length scale of 16 mm, giving a wedge thickness variation of 0–3 nm for Au and 0–6 nm for Cu. For the PIM study a SL thickness wedge was deposited directly onto the CoFe layer with the Pt deposited on top.

For the exploration of interface and SL location effects the Cu or Au was deposited within the successive Pt layers. The specific details of each sample are presented schematically in later sections.

Damping was investigated using FMR measurements carried out at various locations along a thickness wedge using a vector network analyzer (VNA) over both a wide frequency and magnetic field range (up to 40 GHz and 11 kOe, respectively), and measurements were made at room temperature. The FMR signals were fitted to extract the magnetic field linewidths ΔH which are plotted as a function of resonant frequency and modeled with a linear best fit that was interpreted using

$$\Delta H = \frac{4\pi\alpha}{\gamma} f + \Delta H_0, \tag{1}$$

where ΔH_0 is the extrinsic damping term, γ the gyromagnetic ratio, and α is the Gilbert damping parameter that represents the intrinsic damping of the system, which can be enhanced through interfacial effects.

PIM in the Pt and Au layers was investigated using XMCD and XRMR on the 4-ID-D beamline of the Advanced Photon Source at Argonne National Laboratory. These experiments probed the element specific $2p$ to $5d$ electron transitions at the Pt (11.564 keV) and Au (11.919 keV) L_3 edges. The measured XMCD electronic signal was taken as $\frac{I^+ - I^-}{I^+ + I^-}$, where I^+ and I^- denote the spectra recorded with opposite helicity of circularly polarized x rays. The field dependence of the XMCD signal was measured in fluorescence mode using an energy dispersive detector with the field applied in plane. To track the proximity-induced moment as a function of the thickness of the SL, the field-dependent measurements were undertaken as a function of position at 2-mm steps along the SL wedge, the x-ray beam width was 25 μm. The magnetic reflectivity, XRMR, data were taken with an avalanche photodiode detector and an in-plane field of 500 Oe at the Pt and Au L_3 edges. The resonant reflectivity measurements allow simultaneous fitting of the structural and element specific magnetic scattering length densities using the GENX code [55].

SIMS measurements were undertaken to provide compositional depth profiles. Measurements were obtained using a CAMECA SC Ultra system at 4×10^{-10} mbar conditions, with subnanometer depth resolution using a Cs^+ source in primary beam mode and an ultralow impact energy of 100 eV. Measurements were performed in positive secondary ion detection mode and all ions were registered as CsX^+ complex ions. The primary beam was rastered over 250×250 μm^2 while the analysis area was limited to a rectangular region 10×200 μm^2. Note that while the SIMS signals are proportional to the elemental abundance, Fe has a much higher ionization probability, making it appear more abundant than other elements.

III. COPPER SPACER LAYERS

A. Damping and PIM with a Cu spacer layer

The relationship between damping and PIM was explored with a Cu spacer layer thickness wedge between layers of CoFe and Pt of fixed thickness. The multilayer structure

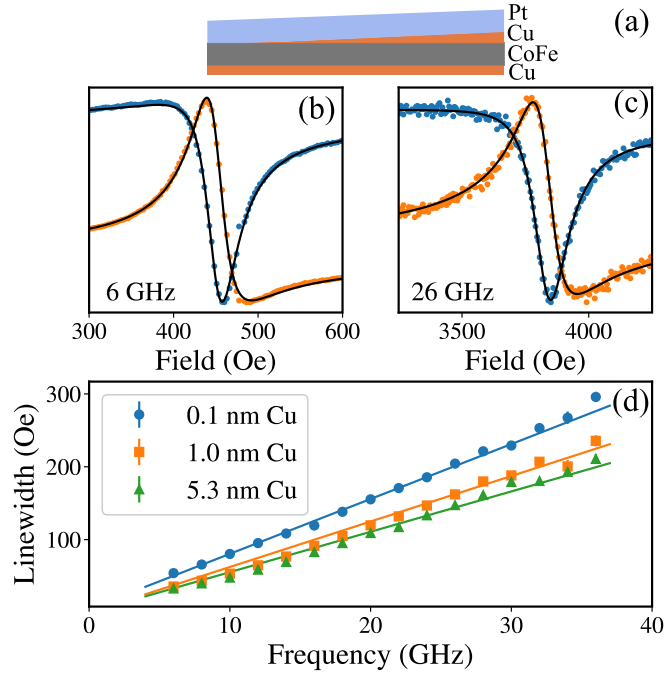

FIG. 1. (a) Schematic showing the sample structure with the Cu spacer layer thickness wedge. (b), (c) Examples of the fitted FMR signals as a function of applied magnetic field at 6 and 26 GHz for a 1-nm Cu SL thickness and (d) representative frequency dependence of the FMR field linewidth with linear fits for three Cu spacer layer thicknesses.

Cu/CoFe(7 nm)/Cu(t)/Pt(10 nm) is shown schematically in Fig. 1(a). Damping was measured as a function of Cu SL thickness. Figures 1(b) and 1(c) show examples of the real and imaginary components of the FMR signal at two excitation frequencies with the best fit lines used to obtain the resonant linewidths. Figure 1(d) shows the linewidths as a function of resonant frequency and the linear best fits analyzed with Eq. (1). The damping of the system is shown as a function of Cu SL thickness in Fig. 2. With increasing Cu thickness the

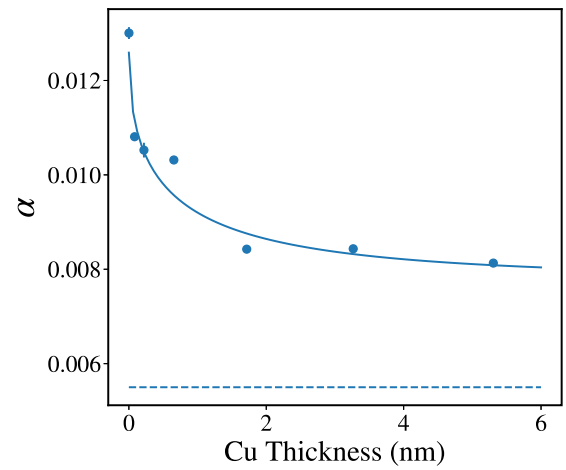

FIG. 2. Gilbert damping parameter as a function of Cu SL thickness for the Cu/CoFe(7 nm)/Cu(t)/Pt(10 nm) system. The horizontal dashed line represents the damping in native CoFe. The solid line is a best fitting exponential function.

damping falls rapidly to a plateau that is significantly above the native CoFe value. To aid analysis, a simple exponential function was fitted to the data, giving a length scale for a drop of $1/e$ of 0.66 ± 0.07 nm. To properly correlate any reduction in the Pt PIM with a reduction of the damping with increasing Cu thickness, it is important to determine the layer thicknesses and interface widths, and both the magnitude and spatial extent of any Pt PIM with the increasing Cu SL thickness. These were probed with XRMR.

Examples of magnetic reflectivity data and best fitting simulations for both the specular reflectivity and the magnetic asymmetry are shown in Fig. 3(a). The resulting structural (sSLD) and magnetic (mSLD) scattering length densities, which represent the physical structure and the element specific Pt magnetization, are shown as a function of depth through the sample thickness in Fig. 3(b). The magnitude of the magnetic asymmetry ratio and the mSLD decrease significantly with the addition of a small nominal Cu thickness between the CoFe and the Pt. The mSLD peak for Pt is reduced by an order of magnitude with a 1-nm SL of Cu between the FM and Pt, while in all cases the induced Pt moment is closely associated with the FM interface within a 2-nm region.

XMCD measurements at the Pt edge were used to determine the Cu SL thickness dependence of the integrated Pt PIM in more detail. Figure 4(a) shows the measured peak Pt XMCD signal, taken at a fixed energy and 500 Oe magnetic field, as a function of Cu SL thickness, which confirms the decrease in the PIM at the onset of the Cu SL. Additionally, element specific hysteresis loops for the Pt were measured as a function of Cu SL thickness across the sample, providing further evidence of the rapid reduction of the Pt PIM with increasing Cu thickness [see Figs. 4(b)–4(d)], the Pt signal being just discernible above the measurement noise for a 1-nm Cu SL thickness.

An exponential fit to the XMCD data in Fig. 4(a) enables a comparison of the Pt PIM with the measured damping in Fig. 2 at equivalent positions on the Cu wedge. Figure 5 shows the damping as a function of Pt PIM in the Cu/CoFe/Cu(t)/Pt system, with Cu thicknesses corresponding to the region measured both for damping and XMCD [the circle points in Fig. 4(a)]. The damping is highest when the PIM is largest, but the relationship between the damping and induced moment is not simple. However, taking into account the dependence of the damping on the Cu spacer thickness introduced previously, it is evident that the change in the damping with the Cu SL does not come solely from a reduction of the interfacial FM/HM d-d hybridization, upon which the PIM is dependent, but is a combination of this orbital hybridization and a reduction in interface transparency, i.e., the spin mixing conductance in the spin-pumping formalism. Significant losses within the Cu due to dephasing of spins are unlikely, because of the weak SOC and the large spin diffusion length of Cu. This is in agreement with the work of Omelchenko *et al.* [44], in that the two contributions are interrelated and not irrelevant.

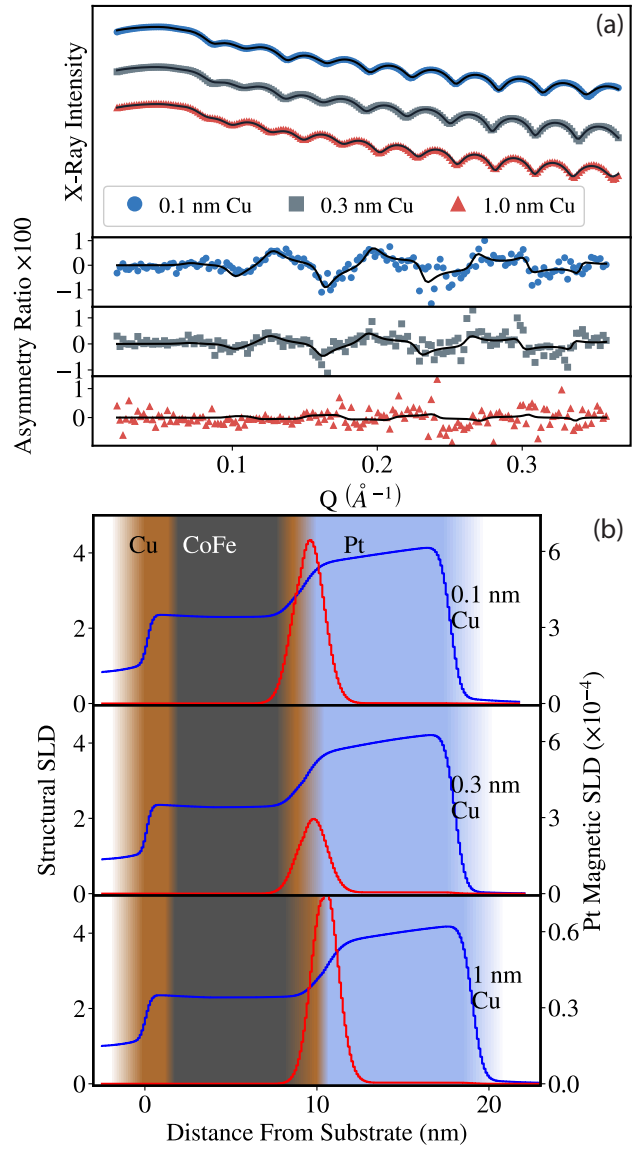

FIG. 3. (a) Magnetic reflectivity profiles at the Pt L_3 edge with corresponding x-ray helicity asymmetry ratio for three nominal thicknesses of Cu spacer layer in a CoFe/Cu/Pt structure. The asymmetry ratio is as defined in the text. The solid lines represent best fitting models to both the structural and magnetic data. (b) Structural (blue) and Pt magnetic (red) scattering length densities from the best fitting simulations to the x-ray reflectivity data for three Cu thicknesses. Note the large change of mSLD-axis scale for the thickest Cu SL.

B. Separating the effects of Pt PIM and the Cu SL interface effects on damping

In an attempt to separate the effects of the Cu layer, additional interfaces, and the Pt PIM on the enhancement of the damping and the spin transport, a comparison was made between a simple FM/Pt (wedge) system and one with a 2-nm-thick Cu SL located halfway through the thickness of a Pt layer wedge, as shown schematically in Fig. 6(a). In both cases a Pt PIM is expected at the FM/Pt interface, while the Cu layer contributes an additional layer and interfaces to the structure. Figure 6(b) shows that for both systems the damping increases and tends to a plateau with increasing Pt thickness up to 10 nm. Notably, the enhancement of the damping is larger in the system with the Cu layer located within the Pt. This is shown quantitatively by plotting the difference in

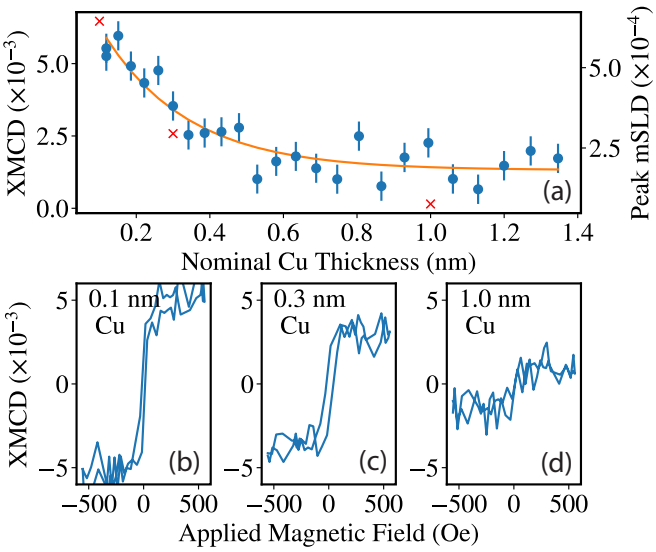

FIG. 4. (a) Measured XMCD peak intensity at Pt L_3 edge as a function of Cu SL thickness (blue dots) in the Cu/CoFe(7 nm)/Cu(t)/Pt(10 nm) system. The solid line shows the best fitting exponential function and red crosses show the peak mSLD data for comparison. (b)–(d) Pt hysteresis loops taken at three Cu thicknesses.

damping between the two systems as a function of the total Pt thickness, which is shown in Fig. 6(c).

The additional damping enhancement with the Cu SL is not constant with Pt thickness, but rises to a peak with 3 nm of Pt and falls, but persists, for thicker Pt. Three factors may contribute to this behavior. The first two factors are length scales, the first being the spin diffusion length λ_{sd} of the Pt spin sink. Spin current propagating into a spin sink is

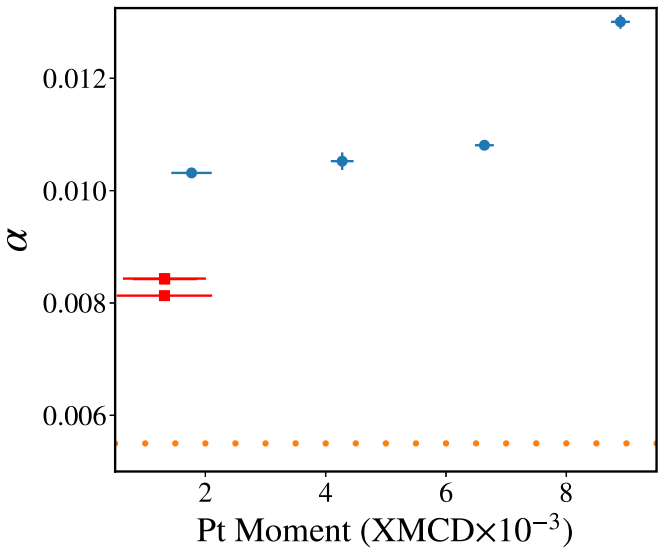

FIG. 5. Damping and XMCD signal for the same Cu spacer thicknesses in the CoFe/Cu(t)/Pt. The circles represent the measured damping values at best fitting XMCD values (from 0 to 2 nm) and the square points represent the damping values for higher Cu SL thicknesses. The dotted line represents the damping of the native CoFe.

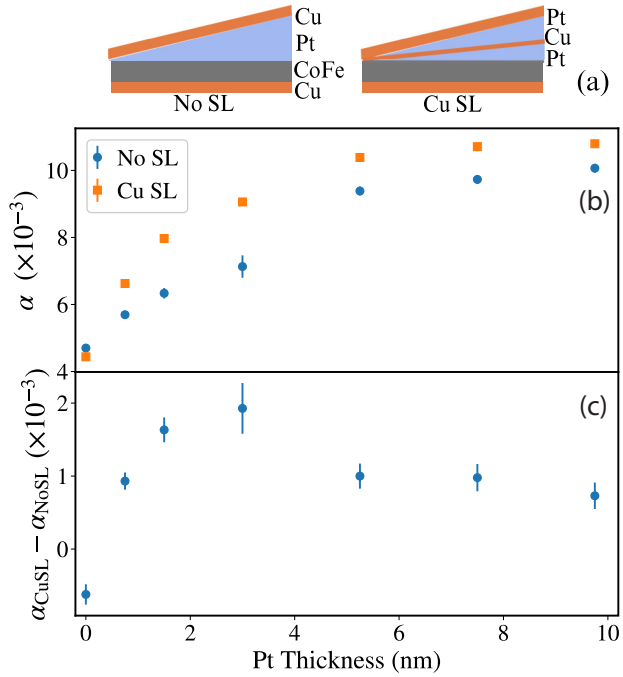

FIG. 6. (a) Schematic of systems with and without a Cu SL within the Pt. (b) Measured damping parameter from the FMR linewidth for Cu(2 nm)/CoFe(7 nm)/Pt[t (nm)] and Cu(2 nm)/CoFe (7 nm)/Pt[$t/2$ (nm)]/Cu(5 nm)/Pt[$t/2$ (nm)] systems. (c) Difference in the damping parameter between the two systems.

subjected to spin-flip scattering over a length scale defined by λ_{sd}. The spin current decays rapidly, falling to $1/e$ within the spin diffusion length. For Pt, λ_{sd} is of the order of several nanometers [6,47,56], so the first few nanometers of Pt are most important for spin current decay. The second length scale is the extent of the interfacial PIM, which, as shown earlier, at around 2 nm is shorter than the spin diffusion length, but is positively related with enhancement of the damping [10]. The third factor is the role of the Cu layer and the associated interfaces with respect to spin current propagation. Since Cu has a long λ_{sd} it is unlikely that significant spin-dependent scattering will occur within the 2-nm Cu layer, suggesting that the additional Pt/Cu interfaces play a key role in the enhanced damping due to enhanced spin-flip scattering at these interfaces, which has been termed spin-memory loss [57]. It has also been suggested that the spin current may be reflected at an interface due to a reduction in the conduction transparency [58]. The combination of these two length scales and the additional interface scattering may account for the nonlinear enhancement of the damping in the Cu SL system compared to that for the simple CoFe/Pt system. For the lowest Pt thicknesses, the Cu layer is very to close to the interface and will disrupt the Pt PIM, which would explain why for the thinnest Pt the addition of Cu actually reduces the damping. For thicker Pt the Cu layer is further away from the interface and will not affect the interfacial PIM. The Pt/Cu interfaces also contribute additional scattering of the pumped spin current that enhances the damping. This interfacial enhancement will be present for all Pt thicknesses, but will be more significant when the additional Pt/Cu interface is closer to the FM and

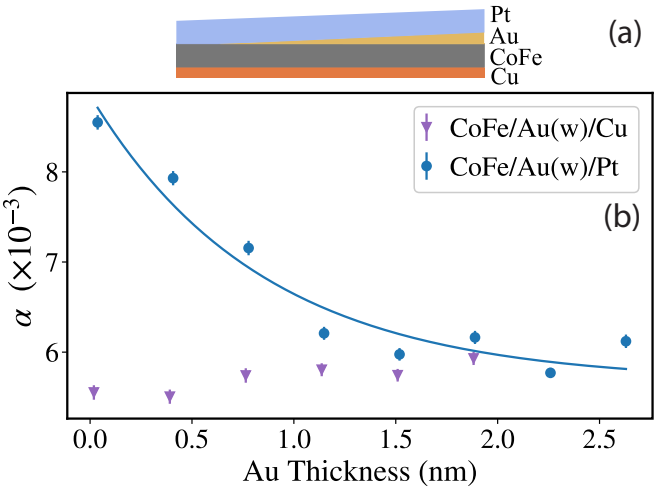

FIG. 7. (a) Schematic illustration of Cu/CoFe/Au(t)/Pt structure. (b) Intrinsic damping contribution α as a function of Au thickness for the multilayers detailed in the legend. The solid line is a best fitting exponential to Cu/CoFe/Au(t)/Pt data.

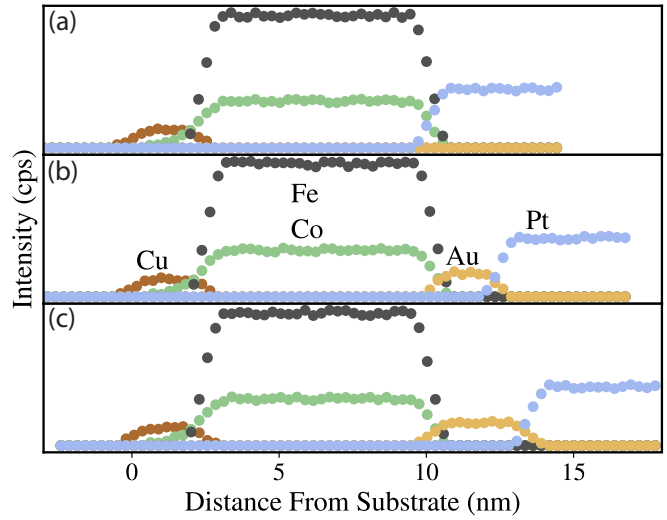

FIG. 8. Secondary ion mass spectroscopy measurements of the Cu/CoFe/Au(t)/Pt system at three locations along the Au spacer layer wedge with (a) 0 nm, (b) 1.5 nm, and (c) 3 nm Au.

will contribute less when the Cu SL is further from the FM/Pt interface, because the spin current decays most rapidly closer to the FM/Pt interface. Hence the difference in damping as a function of Pt thickness between the two systems is initially negative as the Cu disrupts the Pt PIM, reducing the effect on damping, rises to a peak as the PIM is fully established, and the interfacial scattering has a significant role and falls back to a small positive level when the interfacial scattering contributes, but much of the spin current has already dissipated closer the FM/Pt interface.

These results show there is an additional role that the interface plays with regard to damping enhancement, but it is difficult to disentangle interfacial effects and the role of PIM on the damping and interfacial spin transport in this case. Replacing the Cu SL with Au, which has a similar electronic structure to Pt with 5d electrons, but with a reduced ability to hybridize with the FM and a lower SOC compared to Pt [59], enables further investigations of these relationships, as detailed in the following section.

IV. GOLD SPACER LAYERS

A. Damping and PIM with a Au spacer layer

As for the Cu SL sample, a multilayered system was deposited with an increasing thickness of Au deposited directly between the CoFe and Pt layers in a Cu/$Co_{74}Fe_{25}$(7 nm)/Au(t)/Pt(4 nm) structure. A reference multilayer consisting of Cu/CoFe(7 nm)/Au(t)/Cu was fabricated for comparison. Figure 7(a) shows a schematic illustration of the multilayered structure with the Au thickness wedge. The effect of increasing Au SL thickness on the damping parameter α of both systems is shown in Fig. 7(b). The Cu/CoFe/Au(t)/Pt system is similar to the Cu SL case with the damping decreasing rapidly with increasing Au SL thickness before more gradually approaching a constant value beyond ∼1.5-nm Au SL thickness. However, in contrast to the Cu case, the damping of the Au SL system approached the value for the native CoFe. For the reference sample without a Pt spin-sink layer, a small increase in damping was observed with increasing thickness of the Au SL, indicating a very small direct enhancement of the damping with Au.

To understand the observed reduction of the damping with increasing Au thickness, it is helpful to detail the multilayered structure and both the magnitude and spatial extent of the Pt PIM with increasing Au SL thickness. Figure 8 shows the SIMS analysis for different Au thicknesses in the Cu/CoFe/Au/Pt multilayered structure, which shows clearly the distinct layers and the nanometer-scale extent of the interfaces between the layers. Figure 9 shows the measured XRMR profiles and the magnetic asymmetry ratios for various Au spacer thicknesses, at both the Pt and Au L_3 edges, respectively. The data are plotted along with the best fitting simulations. The reduction in the magnitude of the asymmetry ratios at the Pt L_3 edge is, therefore, indicative of a reducing Pt moment as the thickness of the Au spacer layer increases. The resulting sSLD and mSLD obtained from the best fits are shown in Fig. 10 with increasing Au thickness. With no Au present, the induced Pt moment is confined to the interface, as was also observed with the Cu SL samples. However, with increasing Au SL thickness, the magnitude of the Pt PIM peak drops sharply and also broadens away from the interface, while the peak of the Pt moment remains close to the Au/Pt interface.

The overall thickness dependences of the element specific PIM in Pt and in Au are summarized in Fig. 11. These data show the averaged peak amplitudes from the XMCD energy scans measured with a 500 Oe magnetic field, and the peak signal amplitude from element specific hysteresis loops recorded at both the Au and Pt L_3 edges as a function of the Au spacer layer thickness. Hysteresis loops were concurrently fitted with two tanh functions accounting for the positive and negative magnetic field sweeps, with the coercivity, shape, and peak value as variables. The error bars on the hysteresis loops are taken from the raw x-ray counts, and the error bars on

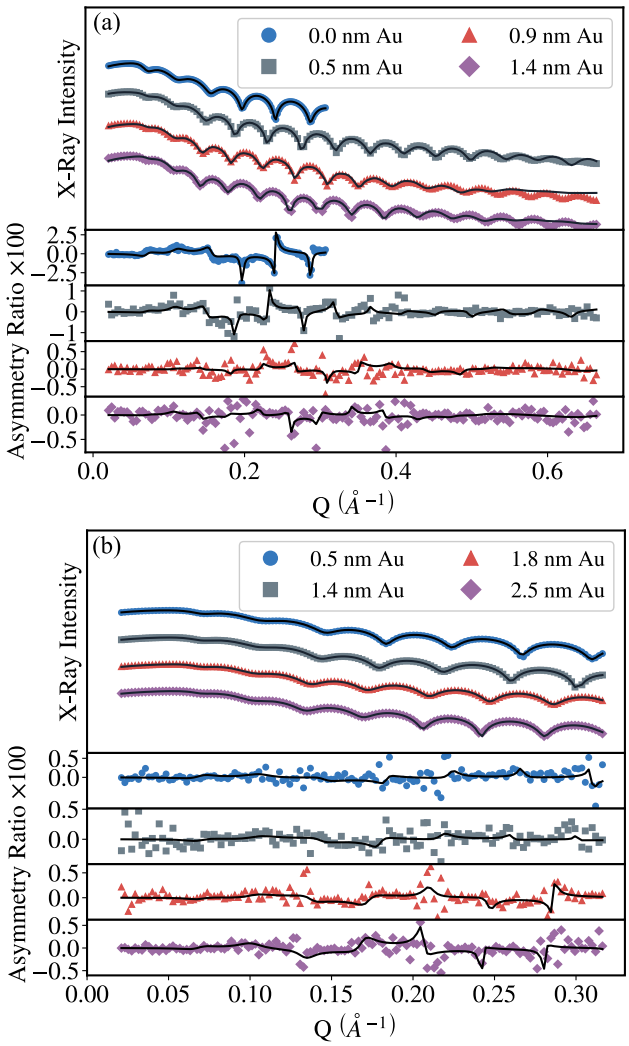

FIG. 9. (a) Measured reflectivity profiles (upper pane) at the Pt L_3 edge with corresponding x-ray helicity asymmetry ratio (lower panes) for four nominal thicknesses of Au spacer layer in a Cu/CoFe/Au/Pt structure. (b) The same measurements at the Au L_3 edge. The asymmetry ratio is as defined in the previous sections. The solid lines represent best fitting models to both the structural and magnetic data.

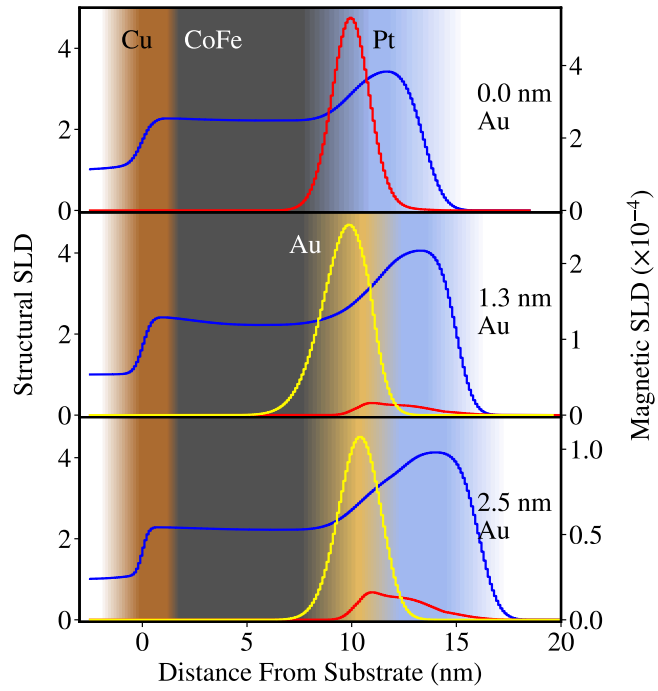

FIG. 10. Structural (blue) and magnetic (red and yellow) scattering length densities from the model fits to the magnetic reflectivity data for varying Au spacer layer thicknesses, indicated on the figure. The red line indicates the extent of the induced Pt moment and the yellow the extent of the induced Au moment. Note the mSLD axes have different scales.

the peak XMCD signals as a function of Au thickness are obtained from the fits to the hysteresis loops. The Pt XMCD signal falls exponentially over a length scale (1.8 ± 0.2 nm) with increasing Au spacer layer thickness, the Pt PIM effectively falling to zero beyond 2 nm of the Au spacer.

The Au XMCD signal and the hysteresis loops show the presence of an induced Au magnetic moment. The XMCD signal rises rapidly with the initial increase in Au thickness, reaching a peak around a nominal 0.5-nm Au thickness before falling back to a constant value for thicker Au. The maximum in the Au PIM at lower thicknesses corresponds to the region where the Au is ultrathin and significantly intermixed with both the CoFe and the Pt, as shown by the XRMR and the SIMS. Considering that the 5*d* states of Au are normally filled there should be little scope for an induced magnetic moment, however, hybridization with a FM produces 5*d* holes, which results in a spin polarization enabling a small induced magnetic moment [20,60,61]. In addition, hybridization of the Pt and Au 5*d* states may increase the holes in Au 5*d* and partially fills the Pt 5*d* orbitals. It is suggested that the local disorder in the ultrathin regime changes the hybridization between the Pt and Au 5*d* states and the FM 3*d* which combines to increase holes in the Au 5*d* states and give rise to the peak observed in the Au PIM.

Returning to the damping and Pt PIM in this system as a function of the Au SL thickness, the exponential fit to the XMCD data in Fig. 11(a) enables a comparison of the Pt PIM with the measured damping in Fig. 7 at equivalent thicknesses of the Au SL. Figure 12 shows the damping as a function of Pt PIM in the Cu/CoFe/Au(t)/Pt system that results from different Au SL thicknesses. This shows a significant, nonlinear correlation between the damping and PIM. The damping is largest when the Pt PIM is largest and the damping falls as the PIM decreases, approaching the uncapped CoFe damping when the Pt PIM falls to zero.

B. Separating the effects of Pt PIM and the location of the Au layer on damping

To separate the effects on damping of the Au SL itself from any changes related to the Pt PIM, the results in the previous section are compared with those from a multilayered structure in which the Au SL thickness wedge was located between two 2-nm-thick Pt layers, so the total Pt thickness was constant and equal to the total Pt thickness of the sample in the previous section, where the Au SL was in contact with

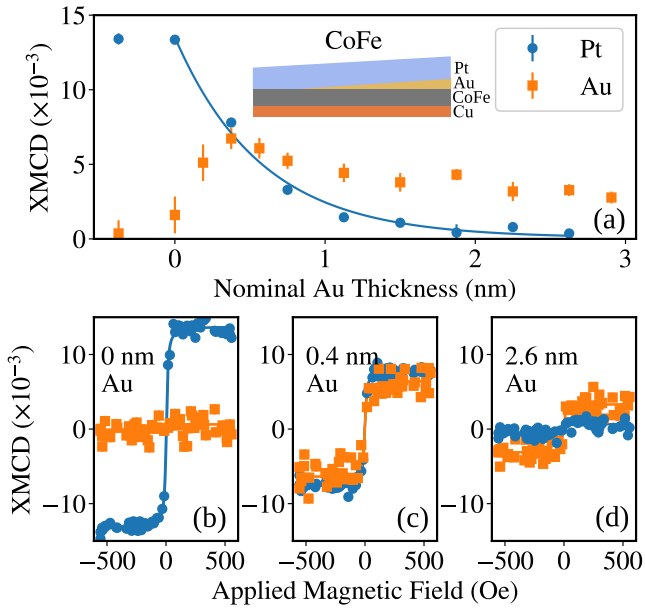

FIG. 11. (a) Measured XMCD as a function of Au spacer thickness at both the Pt (blue) and Au (orange) L_3 edges, with element specific hysteresis loops at three positions across the wedge, for (b)–(d) Cu(2 nm)/CoFe(7 nm)/Au/Pt(4 nm). Solid lines in (a) are best fitting exponential functions.

the CoFe layer. The two multilayered structures are shown schematically in Fig. 13(a). The effect of the Au SL thickness on the damping is shown for both systems in Fig. 13(b). There is almost no change to the damping measured when the Au SL is located entirely within the Pt, except for a small initial offset in the damping linked to the introduction of the Au. The invariance of the damping with Au thickness could indicate (i) the initial 2-nm Pt layer in contact with the CoFe accounts for all the damping enhancement and hence additional Pt beyond

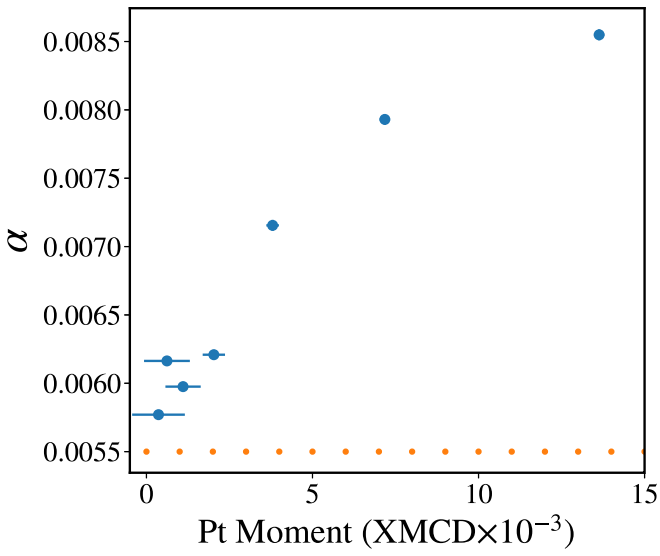

FIG. 12. Damping as a function of XMCD signal for equivalent Au SL thicknesses in Cu/CoFe/Au(t)/Pt. The data points represent the measured damping values at best fitting XMCD values and the horizontal dotted line shows the damping value for the native CoFe.

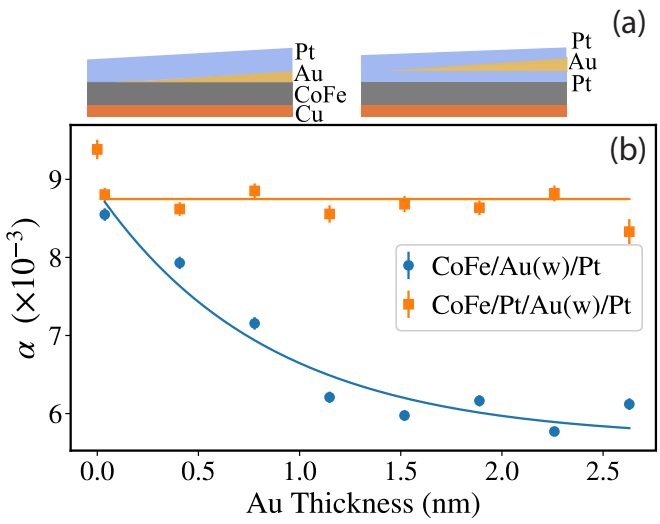

FIG. 13. (a) Schematic illustration of Au SL structures. (b) Intrinsic damping contribution, α, to the FMR linewidth as a function of Au thickness for the multilayers detailed in (a). The solid blue line is a best fitting exponential.

2 nm would play no role, or (ii) the Au intermediate SL is effectively transparent to the spin current when located within the Pt. While case (i) is consistent with the smallest values reported for the spin diffusion length λ_{sd} in Pt [62], it is not supported by other studies, where λ_{sd} in Pt is of order ∼10 nm [6,56], and furthermore it is inconsistent with the increasing α values presented earlier for Pt thicknesses greater than 2 nm (see CoFe/Pt data in Fig. 6, which also indicates that λ_{sd} is greater than 2 nm). So case (ii), based on spin transparency of the Au interlayer, provides a better explanation for this observation.

V. DISCUSSION AND CONCLUSIONS

The results obtained represent a series of multilayered samples that were designed to investigate and separate the effects of PIM and the addition of spacer layers and their interfaces on the damping and the associated spin transport in FM/HM systems. Cu and Au were selected as SL layers for their large spin diffusion length, but otherwise different sizes and electronic structures that provide a contrast with the Pt spin sink and CoFe ferromagnetic layers, respectively.

For the study of correlation between damping and PIM, the SL was placed directly between the FM and HM layers. With increasing thickness of the Cu or Au SL, the damping of the systems and the PIM in the Pt both fall rapidly. With Cu the damping drops to a plateau level that is above the damping of the native CoFe layer, whereas with the Au SL the damping falls to close to the damping of the CoFe film (compare Figs. 2 and 7). In both cases the PIM in the Pt decays rapidly with increasing SL thickness and is very small beyond 1–2 nm of the SL.

The XRMR analysis shows that the Pt PIM is closely associated with the interface to the FM, which has a structural interface width (intermixing and topographical) that is comparable with the extent of the PIM. The introduction of the SL reduces the magnitude of the Pt PIM. For the Cu SL, the Pt

PIM retains a similar spatial profile at the interface, whereas for the Au SL the profile of the Pt PIM broadens, extending further into the Pt layer and the Au also acquires a PIM. The thickness dependence of the Au moment is interesting with the Au PIM initially increasing with Au thickness, before falling back to a lower constant value for thicker Au. This suggests some hybridization of 5*d* states between the Au and the Pt that gives rise to a higher Au PIM for intermixed Au/Pt compared to the pure Au PIM established for thicker Au in contact with the FM.

Exponential fits to the damping and Pt PIM data for the Cu and Au systems enabled the relations between damping and PIM to be obtained. For both spacer layer systems the damping is highest when the Pt PIM is largest and the damping is lowest when the Pt PIM is lost (compare Figs. 5 and 12). Between these extremes the behavior is nonlinear and has a different form for the Cu and Au systems. It is also noted that with a Cu SL the lowest damping is higher than for the native CoFe film, while for the Au SL the lowest damping is close to the CoFe value. These observations demonstrate a correlation between the PIM and damping, but also indicate that the SL material influences the behavior.

As outlined earlier, PIM and the associated Stoner enhancement have no specified role within the spin-pumping formalism for the enhancement of damping, as both the Sharvin conductance and nonequilibrium spin accumulation are unaffected [36]. However, this is not the only contribution to the damping in this model; it is suggested that PIM in the Pt layer increases the ratio of spin-flip to spin-conserving scattering events, and thus modifies the damping. Furthermore, the orbital hybridization that gives rise to PIM [13] may be linked to the damping enhancement in FM/NM systems via the direct electronic interactions across the interface, as shown in the tight-binding analysis of Barati *et al.* that showed the largest contribution to damping originates from the first couple of monolayers of the NM [39]. The experimental evidence for a link between PIM and damping is clear and suggests the need for further theoretical developments to more fully represent the physical basis for enhanced damping in FM/NM systems.

To further investigate the effects of different SLs and their interfaces, damping was measured with Cu or Au where the SL was moved away from the FM/Pt interface and effectively embedded within the Pt layer. This also allowed different aspects of the SL contributions to be explored (as discussed in the Cu and Au sections). In the case of the Cu system, a fixed SL thickness was embedded into a Pt thickness wedge to enable the SL location with respect to the FM interface and the intervening Pt thickness to be varied. In the case of the Au system, the sample design embedded a Au thickness wedge at a fixed Pt thickness away from the interface to study the SL thickness effect. Together these samples also allowed some comparison of Au and Cu SLs located away from the FM/Pt interface. In both cases the Pt PIM is maintained at the FM/Pt interface, but the damping depends upon the details of the SL material within the Pt. For Cu located halfway through the thickness of the Pt layer, the damping is enhanced compared to the simpler FM/Pt system, with the magnitude depending on the location of the Cu layer with respect to the FM interface. For the Au SL located away from the FM/Pt interface the damping is independent of the Au thickness used. These results suggest a greater transparency for spin current through the Au compared to the Cu. Since the spin diffusion length for both Au and Cu is very large compared to their thicknesses it suggests that any difference in spin transparency is associated with the interfaces between the Pt/Cu and Pt/Au. This transparency may be associated with the local ordering and electronic hybridization 3*d*-5*d* in the Cu/Pt case and 5*d*-5*d* for Au/Pt at the interfaces, in agreement with Gupta *et al.* [42]. It is also noted that the Pt thickness dependence observed here and elsewhere [6] shows the damping enhancement depends on the Pt thickness, which is consistent with spin diffusion within the HM in the spin-pumping model.

Together these results highlight the crucial role of both PIM and the nature of the interfaces in the enhancement of damping in FM/NM systems. It is suggested that for spin transport in multilayered systems, both PIM and spin-impedance matched interfaces need to be considered in both fundamental studies and for future exploitation.

The supporting data for this paper are openly available from the Durham University data archive [63].

ACKNOWLEDGMENTS

Funding is acknowledged from EPSRC for C.S. (1771248, Ref. EP/P510476/1) and the Royal Society for D.A. (IF170030). Support is acknowledged for beam time on 4-ID-D at the Advanced Photon Source supported by the U.S. Department of Energy, Office of Science, and Office of Basic Energy Sciences under Contract No. DE-AC02-06CH11357. Travel and subsistence were funded by the U.K. EPSRC XMaS facility. P.K., F.S., and H.G. acknowledge financial support from the National Science Centre Poland through the OPUS funding (Grant No. 2019/33/B/ST5/02013).

[1] M.-H. Nguyen, C.-F. Pai, K. X. Nguyen, D. A. Muller, D. C. Ralph, and R. A. Buhrman, Appl. Phys. Lett. **106**, 222402 (2015).

[2] W. Zhang, W. Han, X. Jiang, S.-H. Yang, and S. S. Parkin, Nat. Phys. **11**, 496 (2015).

[3] C.-F. Pai, Y. Ou, L. H. Vilela-Leão, D. C. Ralph, and R. A. Buhrman, Phys. Rev. B **92**, 064426 (2015).

[4] M. Tokac, S. A. Bunyaev, G. N. Kakazei, D. S. Schmool, D. Atkinson, and A. T. Hindmarch, Phys. Rev. Lett. **115**, 056601 (2015).

[5] S. Azzawi, A. Ganguly, M. Tokac, R. M. Rowan-Robinson, J. Sinha, A. T. Hindmarch, A. Barman, and D. Atkinson, Phys. Rev. B **93**, 054402 (2016).

[6] C. Swindells, A. T. Hindmarch, A. J. Gallant, and D. Atkinson, Phys. Rev. B **99**, 064406 (2019).

[7] M. Weiler, M. Althammer, M. Schreier, J. Lotze, M. Pernpeintner, S. Meyer, H. Huebl, R. Gross, A. Kamra, J. Xiao, Y. T. Chen, H. J. Jiao, G. E. W. Bauer, and S. T. B. Goennenwein, Phys. Rev. Lett. **111**, 176601 (2013).

[8] M. Caminale, A. Ghosh, S. Auffret, U. Ebels, K. Ollefs, F. Wilhelm, A. Rogalev, and W. E. Bailey, Phys. Rev. B **94**, 014414 (2016).

[9] L. J. Zhu, D. C. Ralph, and R. A. Buhrman, Phys. Rev. B **98**, 134406 (2018).

[10] C. Swindells, H. Głowiński, Y. Choi, D. Haskel, P. Michałowski, T. Hase, P. Kuświk, and D. Atkinson, Appl. Phys. Lett. **119**, 152401 (2021).

[11] G. Schütz, M. Knülle, and H. Ebert, Phys. Scr. **1993**, 302 (1993).

[12] G. Schütz, S. Stähler, M. Knülle, P. Fischer, S. Parkin, and H. Ebert, J. Appl. Phys. **73**, 6430 (1993).

[13] F. Wilhelm, P. Poulopoulos, G. Ceballos, H. Wende, K. Baberschke, P. Srivastava, D. Benea, H. Ebert, M. Angelakeris, N. K. Flevaris, D. Niarchos, A. Rogalev, and N. B. Brookes, Phys. Rev. Lett. **85**, 413 (2000).

[14] T. P. A. Hase, M. S. Brewer, U. B. Arnalds, M. Ahlberg, V. Kapaklis, M. Bjorck, L. Bouchenoire, P. Thompson, D. Haskel, Y. Choi, J. Lang, C. Sanchez-Hanke, and B. Hjorvarsson, Phys. Rev. B **90**, 104403 (2014).

[15] R. E. Parra and J. W. Cable, Phys. Rev. B **21**, 5494 (1980).

[16] W. Grange, I. Galanakis, M. Alouani, M. Maret, J.-P. Kappler, and A. Rogalev, Phys. Rev. B **62**, 1157 (2000).

[17] D. Paudyal, T. Saha-Dasgupta, and A. Mookerjee, J. Phys.: Condens. Matter **16**, 2317 (2004).

[18] J. Vogel, A. Fontaine, V. Cros, F. Petroff, J.-P. Kappler, G. Krill, A. Rogalev, and J. Goulon, Phys. Rev. B **55**, 3663 (1997).

[19] F. Wilhelm, P. Poulopoulos, H. Wende, A. Scherz, K. Baberschke, M. Angelakeris, N. K. Flevaris, and A. Rogalev, Phys. Rev. Lett. **87**, 207202 (2001).

[20] F. Wilhelm, M. Angelakeris, N. Jaouen, P. Poulopoulos, E. T. Papaioannou, C. Mueller, P. Fumagalli, A. Rogalev, and N. K. Flevaris, Phys. Rev. B **69**, 220404(R) (2004).

[21] M. Collet, R. Mattana, J.-B. Moussy, K. Ollefs, S. Collin, C. Deranlot, A. Anane, V. Cros, F. Petroff, F. Wilhelm *et al.*, Appl. Phys. Lett. **111**, 202401 (2017).

[22] W. Amamou, I. V. Pinchuk, A. H. Trout, R. E. A. Williams, N. Antolin, A. Goad, D. J. O'Hara, A. S. Ahmed, W. Windl, D. W. McComb, and R. K. Kawakami, Phys. Rev. Materials **2**, 011401(R) (2018).

[23] H. Wu, Q. Zhang, C. Wan, S. S. Ali, Z. Yuan, L. You, J. Wang, Y. Choi, and X. Han, IEEE Trans. Magn. **51**, 4100104 (2015).

[24] M. Valvidares, N. Dix, M. Isasa, K. Ollefs, F. Wilhelm, A. Rogalev, F. Sanchez, E. Pellegrin, A. Bedoya-Pinto, P. Gargiani, L. E. Hueso, F. Casanova, and J. Fontcuberta, Phys. Rev. B **93**, 214415 (2016).

[25] C. Swindells, B. Nicholson, O. Inyang, Y. Choi, T. Hase, and D. Atkinson, Phys. Rev. Research **2**, 033280 (2020).

[26] M. Suzuki, H. Muraoka, Y. Inaba, H. Miyagawa, N. Kawamura, T. Shimatsu, H. Maruyama, N. Ishimatsu, Y. Isohama, and Y. Sonobe, Phys. Rev. B **72**, 054430 (2005).

[27] C. Klewe, T. Kuschel, J.-M. Schmalhorst, F. Bertram, O. Kuschel, J. Wollschläger, J. Strempfer, M. Meinert, and G. Reiss, Phys. Rev. B **93**, 214440 (2016).

[28] R. Rowan-Robinson, A. Stashkevich, Y. Roussigné, M. Belmeguenai, S. Chérif, A. Thiaville, T. Hase, A. Hindmarch, and D. Atkinson, Sci. Rep. **7**, 16835 (2017).

[29] T. Kuschel, C. Klewe, J.M. Schmalhorst, F. Bertram, O. Kuschel, T. Schemme, J. Wollschlager, S. Francoual, J. Strempfer, A. Gupta, M. Meinert, G. Gotz, D. Meier, and G. Reiss, Phys. Rev. Lett. **115**, 097401 (2015).

[30] M. Belmeguenai, Y. Roussigne, H. Bouloussa, S. M. Cherif, A. Stashkevich, M. Nasui, M. S. Gabor, A. Mora-Hernandez, B. Nicholson, O. O. Inyang, A. T. Hindmarch, and L. Bouchenoire, Phys. Rev. Applied **9**, 044044 (2018).

[31] A. Mukhopadhyay, S. Koyiloth Vayalil, D. Graulich, I. Ahamed, S. Francoual, A. Kashyap, T. Kuschel, and P. Anil Kumar, Phys. Rev. B **102**, 144435 (2020).

[32] O. Inyang, L. Bouchenoire, B. Nicholson, M. Tokac, R. M. Rowan-Robinson, C. J. Kinane, and A. T. Hindmarch, Phys. Rev. B **100**, 174418 (2019).

[33] Y. Tserkovnyak, A. Brataas, and G. E. W. Bauer, Phys. Rev. B **66**, 224403 (2002).

[34] Y. Tserkovnyak, A. Brataas, and G. E. W. Bauer, Phys. Rev. Lett. **88**, 117601 (2002).

[35] A. Brataas, Y. Tserkovnyak, G. E. W. Bauer, and B. I. Halperin, Phys. Rev. B **66**, 060404(R) (2002).

[36] Y. Tserkovnyak, A. Brataas, G. E. W. Bauer, and B. I. Halperin, Rev. Mod. Phys **77**, 1375 (2005).

[37] A. Brataas, Y. Tserkovnyak, and G. E. W. Bauer, Phys. Rev. Lett. **101**, 037207 (2008).

[38] K. Ando, Semicond. Sci. Technol. **29**, 043002 (2014).

[39] E. Barati, M. Cinal, D. M. Edwards, and A. Umerski, Phys. Rev. B **90**, 014420 (2014).

[40] J. Kunes and V. Kamberský, Phys. Rev. B **65**, 212411 (2002).

[41] A. Sakuma, J. Phys. D: Appl. Phys. **48**, 164011 (2015).

[42] K. Gupta, R. J. H. Wesselink, R. Liu, Z. Yuan, and P. J. Kelly, Phys. Rev. Lett. **124**, 087702 (2020).

[43] A. Conca, B. Heinz, M. R. Schweizer, S. Keller, E. Papaioannou, and B. Hillebrands, Phys. Rev. B **95**, 174426 (2017).

[44] P. Omelchenko, E. Girt, and B. Heinrich, Phys. Rev. B **100**, 144418 (2019).

[45] K. Wu, J. Mao, Y. Zuo, J. Yun, B. Cui, X. Zhang, Y. Wang, H. Shi, and X. Li, IEEE Trans. Magn. **55**, 4100305 (2019).

[46] S. Yakata, Y. Ando, T. Miyazaki, and S. Mizukami, Jpn. J. Appl. Phys. **45**, 3892 (2006).

[47] J. Bass and W. P. Pratt, Jr., J. Phys.: Condens. Matter **19**, 183201 (2007).

[48] E. Villamor, M. Isasa, L. E. Hueso, and F. Casanova, Phys. Rev. B **87**, 094417 (2013).

[49] Y. Niimi, D. Wei, H. Idzuchi, T. Wakamura, T. Kato, and Y. C. Otani, Phys. Rev. Lett. **110**, 016805 (2013).

[50] T. Kimura, J. Hamrle, and Y. Otani, Phys. Rev. B **72**, 014461 (2005).

[51] J. Okabayashi, T. Koyama, M. Suzuki, M. Tsujikawa, M. Shirai, and D. Chiba, Sci. Rep. **7**, 46132 (2017).

[52] J. King, A. Ganguly, D. Burn, S. Pal, E. Sallabank, T. Hase, A. Hindmarch, A. Barman, and D. Atkinson, Appl. Phys. Lett. **104**, 242410 (2014).

[53] A. Ganguly, S. Azzawi, S. Saha, J. King, R. Rowan-Robinson, A. Hindmarch, J. Sinha, D. Atkinson, and A. Barman, Sci. Rep. **5**, 17596 (2015).

[54] H. Głowiński, F. Lisiecki, P. Kuświk, J. Dubowik, and F. Stobiecki, J. Alloys Compd. **785**, 891 (2019).

[55] M. Björck and G. Andersson, J. Appl. Crystallogr. **40**, 1174 (2007).

[56] C. Stamm, C. Murer, M. Berritta, J. Feng, M. Gabureac, P. M. Oppeneer, and P. Gambardella, Phys. Rev. Lett. **119**, 087203 (2017).

[57] J. C. Rojas-Sánchez, N. Reyren, P. Laczkowski, W. Savero, J. P. Attané, C. Deranlot, M. Jamet, J. M. George, L. Vila, and H. Jaffr'es, Phys. Rev. Lett. **112**, 106602 (2014).

[58] G. Baez Flores, A. A. Kovalev, M. van Schilfgaarde, and K. D. Belashchenko, Phys. Rev. B **101**, 224405 (2020).

[59] M. Zeng, B. Chen, and S. T. Lim, Appl. Phys. Lett. **114**, 012401 (2019).

[60] J. Cable and E. Wollan, Phys. Rev. B **7**, 2005 (1973).

[61] L. Uba, S. Uba, V. N. Antonov, A. N. Yaresko, T. Ślezak, and J. Korecki, Phys. Rev. B **62**, 13731 (2000).

[62] W. Zhang, V. Vlaminck, J. Pearson, R. Divan, S. Bader, and A. Hoffmann, Appl. Phys. Lett. **103**, 242414 (2013).

[63] http://doi.org/10.15128/r1gm80hv40w.